Separation of oil-in-water emulsions using electrospun fiber membranes and modeling of the fouling mechanism

Separation of Oil-in-Water Emulsions Using Electrospun Fiber Membranes and Modeling of the Fouling Mechanism

Looh Tchuin (Simon) Choong[1], Yi-Min Lin[2], Gregory C. Rutledge[1*]

[1]Department of Chemical Engineering, Massachusetts Institute of Technology

[2] Department of Material Science & Engineering, Massachusetts Institute of Technology

[*]Corresponding author. Tel.: +1 617 253 0171; fax: +1 617 258 5766.

E-mail address: rutledge@mit.edu (G. C. Rutledge).

Abstract

Microfiltration of emulsions of oil (dodecane) in water using electrospun membranes of poly(trimethyl hexamethylene terephthalamide) (PA6(3)T) is demonstrated. Rejection of the emulsified dodecane increased from (4.3 ± 0.9)% to (85 ± 5)% when the ratio of droplet diameter to fiber diameter (d_p/d_f) increased from 0.57 ± 0.04 to 2.5 ± 0.4, respectively. The normalized flux (relative to the pure water flux) decreased in proportion to the increase in emulsified oil concentration. The variations observed in flux with time are well-described by models in which the oil fouls the membrane, imparting an additional resistance to transport. The resistivity of the foulant increased with an increase in the concentration of oil in the feed, and grew fastest when d_p/d_f was close to unity. A foulant deposition model is proposed in which the oil droplets form a conformal coating on the fibers. The normalized flux of electrospun membranes was approximately three times higher than that of a commercial phase inversion membrane of comparable bubble point diameter, while exhibiting a similar rejection.

Keywords: Microfiltration, emulsion, fouling, model, electrospinning

1 Introduction

Mining, petrochemical, steel, textile, and food industries produce oily wastewater. The oil can be categorized based on the diameter of the oil droplets as free (> 150 μm), dispersed (20 – 150 μm), or emulsified oil (< 20 μm) [1]. Free oil can be removed readily by skimming because the settling time required is short. Dissolved air flotation (DAF) is used to increase the buoyancy of smaller oil droplets so that the settling time can be reduced. Alternatively, chemicals like coagulants or de-emulsifiers can be added to increase the size of the oil droplet, which also results in a shorter sedimentation time. Nevertheless, these methods are not effective in treating emulsified oil [2]. The most effective way to remove the emulisifed oil is by using membranes. Membrane separation offers higher oil removal efficiency, lower energy cost, and more compact design compared to skimming, DAF, and chemical treatment [1-5].

Electrospun fiber membranes have gained popularity in separations applications as micro- and ultrafiltration media since the late 1990s [6-18]. This popularity is due to the small diameter fibers produced by electrospinning, with fiber diameters down to ~10 nm, which results in high specific surface areas (~100 m^2/g) [19]. In addition to that, electrospun membranes also have low initial solidities (~10%) and highly interconnected pore structures. These pore properties result in high permeability and improved robustness against fouling, i.e. pore space downstream of the clogged area remains usable. The major drawback of electrospun membranes is their low compaction resistance, which may result in lower hydraulic permeabilities at high pressure [18].

The feasibility of using electrospun membranes as microfiltration membranes has been studied using solid particles with a ratio of particle diameter (d_p) to fiber diameter (d_f) ranging from ~0.2 to ~25 [8,9,17]. The rejection of solid particles was generally high (> 90%) for $d_p/d_f > 2$, but it fell to ~50% and ~15% for d_p/d_f equal to 1 and 0.2, respectively [9]. Deposition of particles within the membrane was observed when $d_p/d_f \leq 1$. Electrospun membranes have been tested as microfilters for separating coarse suspensions of oil in water [20], and as part of a composite ultrafiltration membrane to separate of oil-in-water emulsions [10-12, 14-16]. In the latter works, the electrospun membrane served as the support layer for a thin, selective layer whose pores were one to two orders of magnitude smaller than that of the electrospun support. In this work,

electrospun fiber membranes are evaluated as the selective layer for the microfiltration of oil-in-water emulsions. The d_p/d_f of the electrospun membranes used in this work ranged from ~0.5 to ~2.5.

Fouling is the process by which some of the rejected emulsified oil droplets accumulate either within or above the membranes. Fouling can be categorized as reversible (e.g. concentration polarization) or irreversible (e.g. adsorption within membranes) [21]. Herman and Bredee [22] were the first to model fouling, using power law relationships between the rate of filtration and its time derivative to discern differences in filtration mechanism. Hermia subsequently re-derived the well-known "blocking filtration" laws (e.g. cake filtration, standard blocking, complete blocking, and intermediate blocking)), placing them within a common framework, and extending them to power-law fluids [23]. However, it is generally recognized that these relationships must be used with caution, because fouling is rarely the result of only one mechanism [22, 24]. The fouling of micro- and ultrafiltration membranes are often characterized by the membrane fouling index (MFI), in which the decline in flux is attributed to the specific resistance of the foulant [25-27]. The MFI model assumes that the total resistance to flow is the sum of the resistances of the foulants and that of the membrane (i.e. resistances in series), and that the foulants are rejected above the membranes. In this work, we compare several fouling models with resistance in both series and parallel. We also propose a mechanism for the deposition of foulants within electrospun fiber membranes.

2 Models of Fouling

2.1 Foulant resistivity models

Here we briefly derive a set of models based on classical principles in which the accumulation of foulant modifies the resistance to the flow of liquid through the membrane, acting either in series or parallel with the membrane resistance. If the foulant is assumed to accumulate external to the membrane, it imparts a resistance in addition to that of the membrane. If the foulant accumulates within the membrane, it also modifies the original membrane resistance by reducing its effective volume. These extremes of external and internal fouling may be loosely interpreted as representative of cake filtration and depth filtration, respectively. In cake filtration, the rejection mechanism is size exclusion, where the rejected foulant forms a layer above the membrane. In

depth filtration, the foulant is removed by adsorption onto surfaces within the pores of the membrane. We discriminate between fouling models on the basis the foulant resistivity, which is evaluated as a fitting parameter to data for flux versus time. The foulant resistivity, like specific resistance, is expected to be an intrinsic property of the foulant and therefore insensitive to emulsion concentration or operating conditions.

2.1.1 Resistances in series (RS)

The fouling of a membrane with the resistances in series is illustrated in Figure 1 (a). The flux (J) is identical through the foulant and membrane layers, but the total pressure drop (ΔP) across the membrane is the sum of pressure drops in each layer. Using Darcy's law, the total pressure drop is:

$$\Delta P = J\Delta z_1 \mu R_1 + J\Delta z_2 \mu R_2 \tag{1}$$

where μ is the dynamic viscosity of the liquid, Δz_i is the thickness and R_i is the resistivity of layer i, and the subscripts 1 and 2 refer to the membrane and the foulant, respectively. Using $\Delta z = \Delta z_1 + \Delta z_2$, the expression of the overall flux can be obtained by rearranging Eq. 1.

$$J = \frac{1}{\mu}\left[\frac{1}{R_1 \Delta z_1 / \Delta z + R_2 \Delta z_2 / \Delta z}\right]\frac{\Delta P}{\Delta z} \tag{2}$$

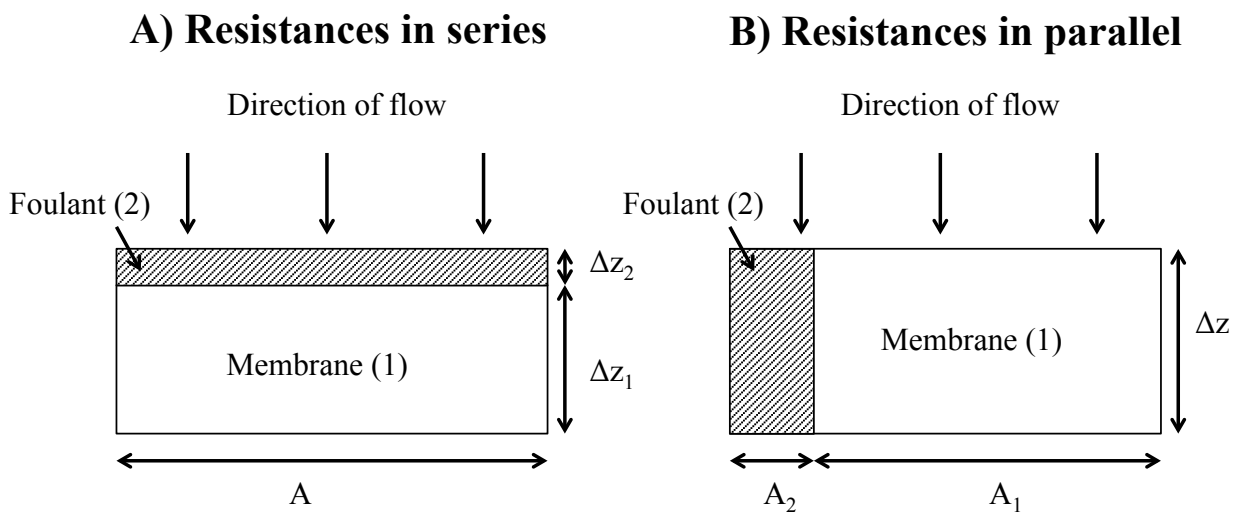

Figure 1 The schematics of the fouling models with resistances in series (a) and in parallel (b).

RS-External (RSE)

If we assume that the fouling of a membrane with resistances in series occurs external to the membrane, we recover the conventional MFI fouling model [25]. To show this, let $\Delta z_1/\Delta z = 1$ and $\Delta z_2/\Delta z = f$, where f is the volume of foulant accumulated on the membrane relative to the membrane volume. That is:

$$f = \frac{m_c}{\rho_{oil} V_m} \tag{3}$$

where V_m is the volume of the membrane, ρ_{oil} is the density of the foulant, and m_c is the mass of the foulant accumulated on the membrane. m_c can in turn be found by a mass balance for the foulant around a section of the membrane, assuming that all of the oil that arrives at the membrane on the feed side is either retained by the membrane or passes through with the permeate:

$$m_c = \int_0^t J(t')\left[C_f - C_p(t')\right] A\, dt' \tag{4}$$

where *J(t)* is the time-dependent flux, C_f is the concentration of foulant in the feed, which is assumed to be constant, $C_p(t)$ is the time-dependent concentration of foulant in the permeate, and *A* is the area of the membrane. The expression for flux after normalization using the pure water flux (J_0) is:

$$\frac{J}{J_0} = \left[1 + f\frac{R_2}{R_1}\right]^{-1} \tag{5}$$

RS-Internal (RSI)

If we instead assume that the fouling of a membrane with resistances in series occurs internal to the membrane, then part of the membrane is modified, or occupied, by the foulant, and the fractional contributions of the membrane and the foulant can be expressed as $\Delta z_1/\Delta z = 1 - f$ and $\Delta z_2/\Delta z = f$. The equation for the normalized flux then becomes:

$$\frac{J}{J_0} = \left[1 + f\left(\frac{R_2}{R_1} - 1\right)\right]^{-1} \tag{6}$$

By equating Eq. 5 and Eq. 6, the following relation is obtained between the foulant resistivities predicted by the RSE and RSI models:

$$R_{2,RSI} = R_{2,RSE} + R_1 \tag{7}$$

From this result, it is apparent that the two models are equivalent when $R_2 >> R_1$. In the absence of additional information about the resistivity of the foulant, it is difficult to discriminate between these two models based on permeation data alone.

2.1.2 Resistances in parallel (RP)

The fouling of a membrane with the resistances in parallel is illustrated in Figure 1 (b). In this case, the pressure drop is the same across both the membrane and the foulant, while the total

volume flow (Q) is the sum of the volume flows through the membrane (Q_1) and through the foulant (Q_2). Using the fact the volume flow is the product of the flux and the membrane area, $Q=JA$, one can write:

$$J = \frac{1}{\mu}\left[\frac{A_1}{AR_1} + \frac{A_2}{AR_2}\right]\frac{\Delta P}{\Delta z} \tag{8}$$

where A is the total membrane area.

RP-External (RPE)

Similar to the RSE analysis, if we assume that fouling occurs external to the membrane, the ratios of A_1/A and A_2/A are 1 and f, respectively. The expression for normalized flux can be written as:

$$\frac{J}{J_0} = 1 + f\frac{R_1}{R_2} \tag{9}$$

By inspection, one can conclude that this fouling model is unlikely. The flux increases as fouling increases, which contradicts the experimental observations [24] and the notion of "fouling". This model is more appropriate for cases where the component accumulated facilitates transport, rather than hinders it. This model is presented for completeness, but not considered further here.

RP-Internal (RPI)

Analogous to the RSI model, we assume that the fouling of a membrane with resistances in parallel occurs internal to the membrane, such that the fractional contributions A_1/A and A_2/A are $1–f$ and f, respectively. The normalized flux according to this model has the following expression:

$$\frac{J}{J_0} = 1 + f\left(\frac{R_1}{R_2} - 1\right) \tag{10}$$

This model can describe fouling in cases where $R_2 > R_1$, such that flux declines as f increases.

Each of these models predicts a linear relationship between J/J_0 (RP models, Eq 9 and 10) or its inverse (RS models, Eq 5 and 6) and the relative volume of accumulated foulant (f), from which the best estimate of R_2/R_1 can be determined, as well as the R-square value that describes the quality of fit. In the terminology of "blocking" models [23, 28], the RSE model corresponds to "cake filtration" ($dJ/dt \sim J^3$), while the RPI model corresponds to "complete blocking" ($dJ/dt \sim J$); these models represent the extremes of filtration behavior.

2.2 Conformally Coated Fibers (CCF) model

The classical series and parallel resistance models can provide some insight into the contributions of foulants to the overall resistance to flow, but they are not specific to fibrous membranes and are not based on any specific physical mechanism of fouling. In this section, we present a model wherein the foulants are assumed to form a uniform coating that envelops the fibers that make up the membrane, both reducing the available volume of the membrane for transport and increasing the effective diameter of the fibers, as shown in Figure 2. We have previously shown that the permeability of electrospun fiber membranes is reasonably well-described by Happel's equation for solidities up to 50-60% [18, 29]. The normalized flux can be approximated by the following equation:

$$\frac{J}{J_0} = \frac{K}{K_0} = \frac{D^2 \phi_0 g(\phi)}{D_0^2 \phi g(\phi_0)} \quad \text{where} \quad g(\phi) = -\ln\phi + \frac{\phi^2 - 1}{\phi^2 + 1}, \tag{11}$$

where K is the permeability (or $1/R$) of the electrospun membrane, ϕ is the solidity of the membrane (solidity=1–porosity) and D is the fiber diameter. With $D/D_0 = (\phi/\phi_0)^{1/2}$, Eq. 11 can be simplified to the following equation:

$$\frac{J}{J_0} = \left(\frac{\phi_0^2 + 1}{\phi^2 + 1}\right)\left[\frac{-\ln\phi - \phi^2 \ln\phi + \phi^2 - 1}{-\ln\phi_0 - \phi_0^2 \ln\phi_0 + \phi_0^2 - 1}\right] \tag{12}$$

This fouling mechanism model, which we call the "conformally coated fibers" (CCF) model, differs qualitatively from the simpler series and parallel resistance models in two important ways: a) the CCF model provides a physical interpretation of the deposition of foulants and the increase in the resistance to flow; b) the resistivity of the foulant in the CCF model is assumed to be infinite i.e. impermeable to the liquid, and is not treated as an adjustable parameter to be determined from the data.

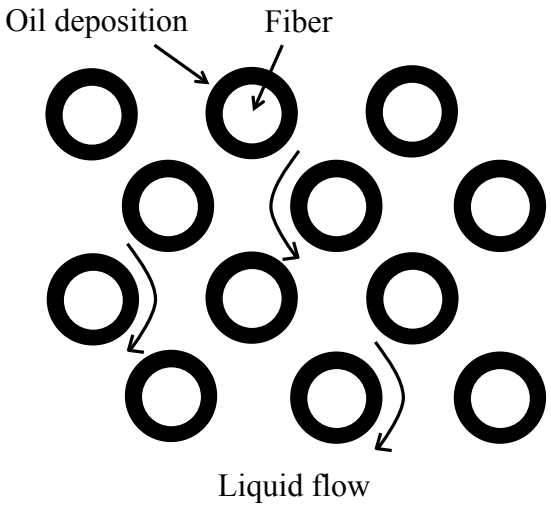

Figure 2 Schematic of the conformally coated fibers (CCF) fouling mechanism for electrospun membranes (fibers are viewed end-on). Arrows are illustrative of streamlines in flow.

3 Experimental

3.1 Materials

Poly(trimethyl hexamethylene terephthalamide) (PA6(3)T), purchased from Sigma Aldrich, is a glassy amorphous solid at room temperature, with a glass transition temperature of 151 $^{\circ}$C, as measured by Differential Scanning Calorimetry (DSC, TA Q100). N,N-dimethyl formamide (DMF) was obtained from Sigma-Aldrich and used as received, as solvent for preparing the PA6(3)T solutions for electrospinning. 2% formic acid (FA) by weight was added to DMF to increase the electrical conductivity. A commercial phase inversion nylon 6,6 membrane (NY4513100) was purchased from Sterlitech, and used as is.

3.2 Fabrication

A vertically aligned, parallel plate setup was used for electrospinning, as described elsewhere [18]. The top plate was 15 cm in diameter and charged with a high voltage supply (Gamma High Voltage Research, ES40P) to a voltage in the range of 25-35 kV. The grounded bottom plate, which also served as the collector for the fiber membrane, was a 15 cm x15 cm stainless steel platform. The tip-to-collector distance was varied from 25 to 35 cm by adjusting the height of the bottom plate. The polymeric solution was loaded into a syringe attached by Teflon tubing to a stainless steel capillary (1.6 mm OD, 1.0 mm ID) that protruded 21 mm through the center of the top plate. A digitally controlled syringe pump (Harvard Apparatus, PHD 2000) was used to control the flow rate of the polymer solution in the range of 0.001-0.003 mL/min. The fiber diameters of the membranes were varied by changing the concentration of PA6(3)T. All the membranes were thermally annealed at 150 $^{\circ}$C for an hour, as described previously, in order to improve the compaction resistances of the membranes [18].

3.4 Membrane characterization.

The average fiber diameter of the electrospun fiber membranes was calculated from the measurement of 30 to 50 fibers in images taken with a scanning electron microscope (SEM, JEOL-JSM-6060). The solidity was calculated gravimetrically, in which the membrane thickness was measured using an adjustable measuring force digital micrometer (Mitutoyo, Model CLM 1.6”QM) with a contact force of 0.5 N.

3.5 Emulsion generation and characterization.

Five percent by volume or 50,000 ppm of dodecane in an 8 mM aqueous solution of sodium dodecyl sulfate (SDS) solution was sonicated using a tip sonicator (Branson Sonifier, 450/101-063-198) at 20% duty cycle, power setting of 3 for five minutes. The concentrated dodecane emulsion was then diluted with MilliQ water, and used as feed. The sizes of the emulsified oil droplets in all streams (feeds, permeates, and retentates) were measured using a dynamic light scattering (DLS) analyzer (Brookhaven Instruments Corp., Zeta PALS). Three replicates were taken for each DLS measurement of a sample, and each replicate measurement lasted for 10 minutes for better reproducibility.

3.6 Separation flux and rejection.

The separation test was performed using a stirred dead-end filtration cell (Sterlitech, HP4750). The cell was oriented vertically with a column of liquid above the membrane. The membranes were sealed by an o-ring. A mask with an opening of 10 mm in diameter was used to reduce the filtration area so that the flow rates were more manageable for accurate measurement of the flux. A feed volume of 40-60 ml was used for each run. The permeate mass was measured as a function of time, in sampling intervals. The permeate mass was converted to volume using the density of water since the concentration of dodecane was low (< 0.05 vol%). The permeate was collected in volumes of at least 1-2 ml, from which the flux and oil concentration for that interval were determined. A new vial was used for each sampling interval. The pure water flux of each membrane was measured at the same operating conditions as used in the separation test, immediately prior to the test. All the membranes were conditioned using pure water flow at 4 psi, the highest pressure used in any of the tests reported here, before measuring the pure water flux. The rejection of dodecane was calculated using the following equation:

$$R(\%) = \left(1 - \frac{C_p}{C_f}\right) \times 100 \tag{13}$$

The oil concentrations were determined using a total organic carbon (TOC) analyzer (Shimadzu TOC-L). Since a minimum volume of 5 ml is required for a TOC analysis on a sample, aliquots of 0.5 ml were diluted ten fold to a final volume of 5 ml using MilliQ water. A calibration curve with TOC concentration ranging from 1 ppm to 100 ppm was obtained using a 200 ppm potassium hydrogen phthalate (KHP) standard solution. Parafilm was used to seal the test vials to minimize change in concentration due to evaporation.

4 Results

4.1 Membrane characterization.

PA6(3)T fiber membranes having three different average fiber diameters, i.e. (99 ± 17) nm, (223 ± 29) nm, and (442 ± 35) nm, were electrospun. SEM images for each fiber diameter are shown

in Figure. 3. The solidities of the membranes were similar, ranging from (10 ± 0.6)% to (13.6 ± 0.5)%. The effective pore sizes of electrospun fiber membranes have been shown both theoretically [30] and experimentally [17,31,32] to be proportional to fiber diameter for membranes of comparable solidity, as is the case in this work. Conventional methods like mercury porosimetry and capillary flow porometry yield average pore sizes estimates that range from 3.5 to 5 times the average fiber diameter, depending on the measurement technique used.

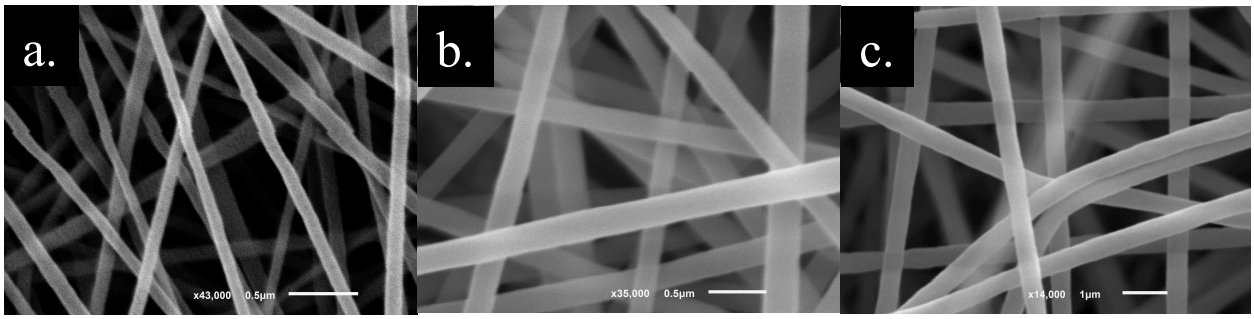

Figure 3 SEM images of electrospun PA6(3)T membranes with average fiber diameter of (a) (99 ± 17) nm; (b) (223 ± 29) nm; and (c) (442 ± 35) nm. The scale bars are 0.5 μm for (a) and (b), and 1 μm for (c).

4.2 Flux.

The effects of operating pressure, emulsion concentration and fiber diameter on the separation properties of electrospun PA6(3)T membranes were studied. Several runs at different combinations of those parameters are documented in Table 1. Parameters like pressure and fiber diameter also affect the hydraulic flux; thus, the permeate flux was normalized by the pure water flux measured for the same membrane and operating pressure (Figure 4 (a)) in order to isolate just the effect of the emulsion on the flux under different conditions. As shown in Figure 4 (b)-(d), the normalized flux decreased with filtration time. The normalized flux also decreased with increase in operating pressure, especially at early times in the filtration process (<100 s). However, the flux was most sensitive to the emulsion concentration. An increase in the concentration led to a proportional decrease in the normalized flux, as shown in Figure 4 (c). The membrane with d_p/d_f = 2.5 (run F) had a higher normalized flux, despite a lower pure water flux than that of the membrane with d_p/d_f = 1.1 (run A).

Table 1 The membrane properties, emulsion properties, and operating pressures for the experiments performed using electrospun PA6(3)T membranes.

Run ID	Operating pressure (psi)	Dodecane emulsion concentration (ppm)	Fiber diameter (nm)	d_p/d_f ratio	Solidity (%)	Membrane thickness (μm)
A	2	500	223 ± 29	1.1 ± 0.1	12.1 ± 0.4	73 ± 5
B	1	500	223 ± 29	1.1 ± 0.1	12.7 ± 0.8	56 ± 7
C	4	500	223 ± 29	1.1 ± 0.1	10.0 ± 0.6	72 ± 1
D	2	100	223 ± 29	1.1 ± 0.1	10.5 ± 0.2	80 ± 2
E	2	1000	223 ± 29	1.1 ± 0.1	13.6 ± 0.5	59 ± 3
F	2	500	99 ± 17	2.5 ± 0.4	10.7 ± 0.3	117 ± 4
G	2	500	442 ± 35	0.57 ± 0.04	10.4 ± 0.4	67 ± 4

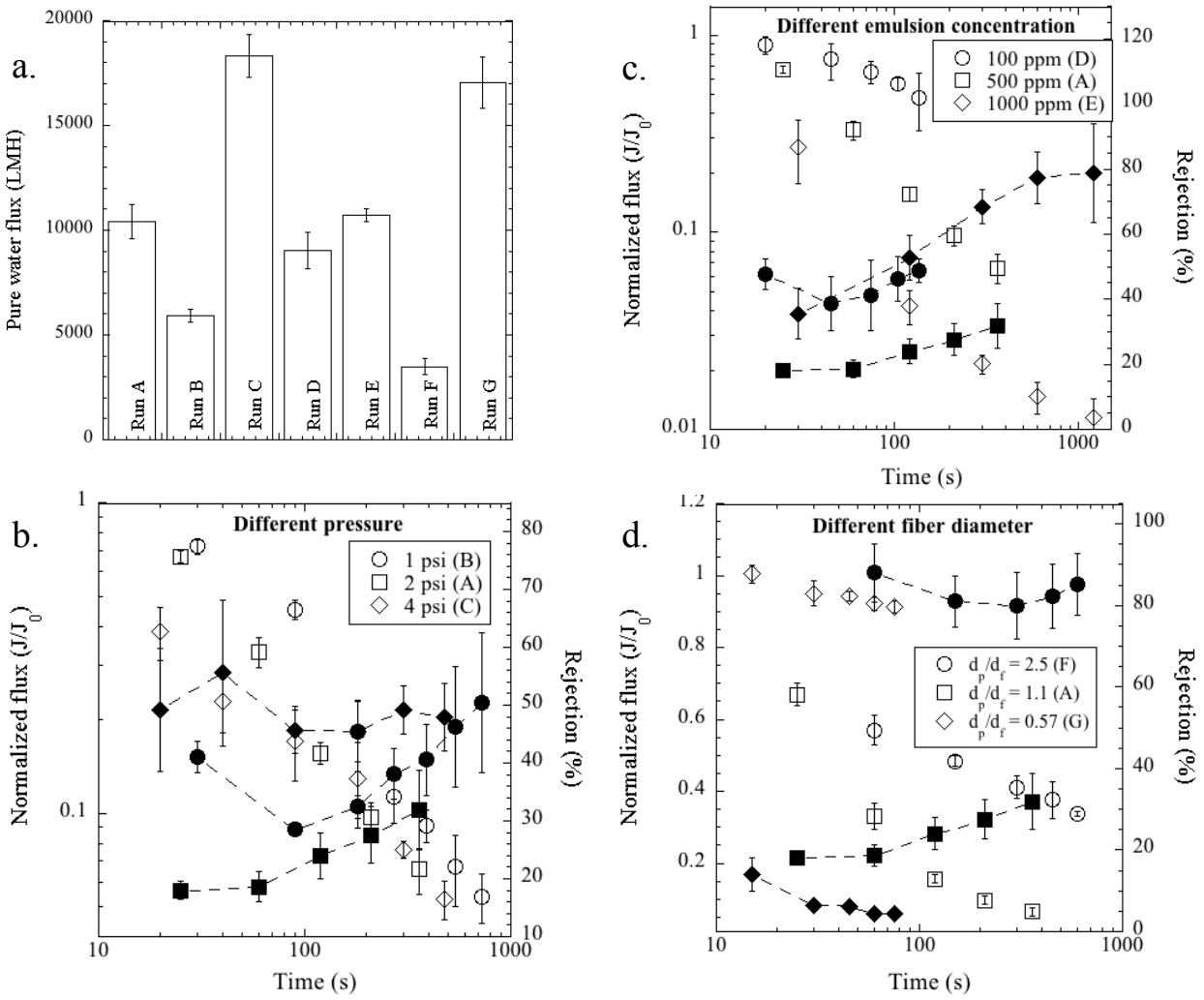

Figure 4 (a) Pure water flux for each run. (b)-(d) The separation properties, i.e. normalized flux (open symbols) and rejection (filled symbols) of dodecane, of electrospun PA6(3)T at different operating pressures (b), concentrations of emulsion (c), and fiber diameters (d). The fluxes are normalized in each case by the pure water flux measured for the same membrane and operating pressure. Run ID's are shown in parentheses (*c.f.* Table 1)

4.3 Rejection

The rejection generally increased with time, as shown in Figure 4 (b)-(d). The rejection was initially higher (t < 100 s) for the higher operating pressure (4 psi) but the rejection at different pressures became similar (~50%) at long filtration time. The rejection was lower for the 500 ppm

feed (run A) than for either the 100 ppm feed (run D) or 1000 ppm (run E). The rejection increased from ~4% to ~85% with an increase in the d_p/d_f ratio from 0.57 to 2.5.

4.4 Emulsion size

The average diameter of the oil droplets in the feed was (250 ± 9) nm. After separation, the distributions of droplet diameter in the permeates of all the runs were broader than that of the feed. The average diameter of the oil droplets increased for the permeates of runs A, B, and D. The average diameter of the droplets decreased by 24 nm and 45 nm for runs C and F, respectively. The diameters of the oil droplets did not change significantly for runs E and G after separation. The oil droplet diameter for the retentate was also measured, and found to be unchanged from that of feed. In runs E and F, a visible oil layer was observed to form on top of the retentate. This oil layer was attributed to a few large drops that detached from the membrane after significant fouling and rapidly rose to the surface of the retentate; this oil layer does not affect subsequent separation, but was included in the determination of total oil content of the retentate.

Table 2 The diameters of the oil droplets measured by dynamic light scattering (DLS).

Sample	Droplet diameter measured by DLS (nm)
Feed	250 ± 9
Permeate of run A	271 ± 20
Permeate of run B	268 ± 36
Permeate of run C	226 ± 11
Permeate of run D	265 ± 17
Permeate of run E	257 ± 36
Permeate of run F	205 ± 16
Permeate of run G	240 ± 18

4.5 Comparison with a commercial membrane.

The separation properties of a commercial phase inversion nylon 6,6 membrane with a nominal bubble point diameter of 0.45 μm are compared with those of run F, in which the electrospun

membrane used had a bubble point diameter of (0.42 ± 0.1) μm. The bubble point diameter was measured by Porous Materials Inc. (PMI, Ithaca NY) using capillary flow porometry. The rejection of run F was comparable to that of the commercial membrane at t < 200 s; but at 600 s, the rejection of run F was approximately 10% higher than that of the commercial membrane, as shown in Figure 5. However, the normalized flux of run F was approximately three times that of the commercial membrane. This increase in flux can be attributed to the difference in the pore structures of the membranes. Electrospun membranes have a more open and interconnected pore network; thus, the pore space downstream of a blockage is still accessible, and the membrane is less sensitive to fouling.

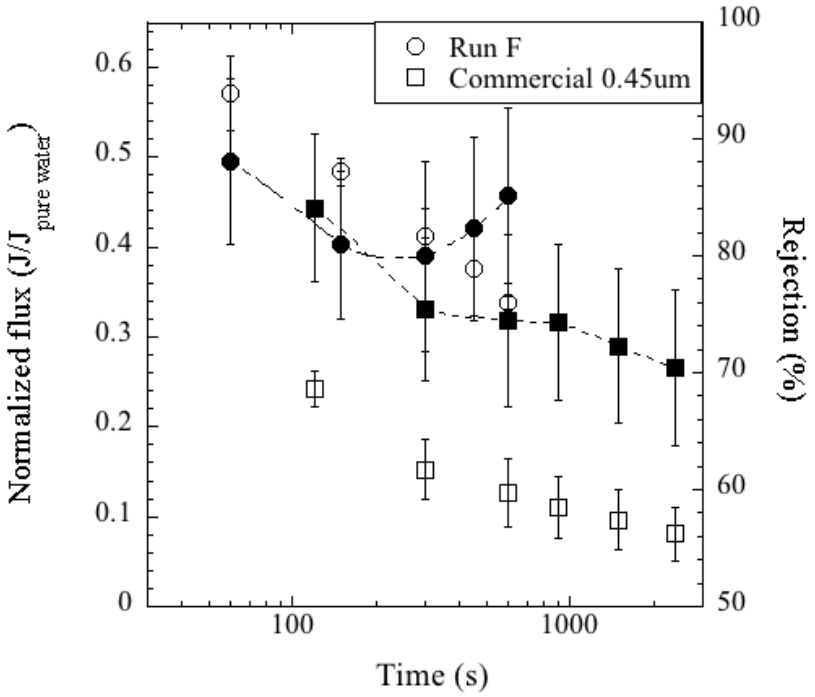

Figure 5 The comparison of the normalized flux (open symbols) and the rejection (filled symbols) between a commercial phase inversion nylon membrane and an electrospun PA6(3)T membrane of comparable bubble point diameter (run F). The pure water flux (J_0) for the commercial membrane was (2500 ± 400) L/m^{2}h, compared to (3500 ± 400) L/m^{2}h for run F.

4.6 Foulant resistivity

Figure 6 shows the resistivity of the clean membranes (R_1), determined from the pure water flux according to Darcy's law, and the resistivity ratios (R_2/R_1) obtained for each run and sampling

interval. (The temporal evolutions of f and C_p for each run can be found in the Supporting Information.) The clean membrane resistivities range from 0.5 to 2.0 x10^{14} m^{-2}. Inspection of Figure 6 indicates that the RPI model generally provides a poor description of the fouling phenomenon for runs A through E (since $R_2/R_1 < 0$), while the RSE and RSI models are indistinguishable for these runs (since $R_2/R_1 >> 1$). For runs F and G, the foulant resistivities are lower than those obtained for runs A-E, and are comparable for the RSI and RPI models. It is worth noting that runs F and G employed membranes produced under different conditions (to increase or decrease the average fiber diameter and pore size) than runs A-E. The R_2 values of the RS models are relatively insensitive to operating pressure (runs A-C), but change by an order of magnitude with a similar change in the oil concentration (runs D, E).

The best estimates of foulant resistivity (R_2) were calculated from linear regressions of J_0/J (for RSE and RSI, Eq 5 and 6) or J/J_0 (for RPI, Eq 10) versus f, subject to the constraint that $J/J_0=1$ for $f=0$ (*c.f.* Supporting Information). The results, and the R-squared values of the linear regressions, are tabulated in Table 3. The R-squared values for RSE and RSI models are identical. The goodness of fit does not discriminate whether the fouling occurred internally or externally. Fouling may occur in both ways. A direct measurement of the R_2 value is needed to determine which RS model is preferred. The R-squared values of the RS models are higher than those of the RPI model for all the runs except runs D and G, where the R-squared values were comparable for all three models, and run F where the poor quality of the linear regressions suggest that R_2 is not constant in this case. The RPI model appears to be applicable only in those cases where the accumulation of foulant within the membrane was small (runs D and G). The RPI model might work in these cases because of the complex, interconnected nature of flow paths around fouled regions within the membrane. However, in most cases, the RPI model produced negative resistivity values (runs A-E), which appear to be aphysical for emulsions of dodecane in water.

The RSI and RPI models assume implicitly that the volume of oil accumulated in the membrane should not exceed the volume of the membrane itself ($f \leq 1$). Nevertheless, use of Eqs (3) and (4) results in f values greater than 1 for several runs, as shown in Table 4. This could be indicative of either a breakdown of the models, or rejection of a portion of the oil back to the

feed during the run. To test the latter, the oil concentration in the retentate at the end of each run was measured and compared to the starting feed concentration. There does not appear to be any strong correlation between cases where $f > 1$ and increases in retentate oil concentration.

Table 3 Foulant resistivities R_2 and the R-square of their linear regression for each model.

Run	R_2 x10^{-15} (m^{-2})			R-squared	
	RSE model	RSI model	RPI model	(RSE, RSI)	(RPI)
A	1.7 ± 0.1	1.7 ± 0.1	-0.044 ± 0.003	0.82	0.38
B	1.0 ± 0.1	1.0 ± 0.1	-2.6 ± 0.3	0.64	0.54
C	1.1 ± 0.1	1.1 ± 0.1	-0.63 ± 0.08	0.82	-7.3
D	0.31 ± 0.04	0.38 ± 0.05	-0.043 ± 0.005	0.73	0.71
E	5.5 ± 0.5	5.6 ± 0.5	-4.2 ± 0.6	0.69	-14
F	0.22 ± 0.03	0.43 ± 0.05	0.37 ± 0.05	-0.12	-5.9
G	0.013 ± 0.002	0.038 ± 0.005	0.047 ± 0.007	0.46	0.46

Table 4 The total volume of foulant with respect to the volume of membrane, f, and the percent change in the concentration of the feed at the end of the separation experiment

Run	f at the end of experiment	Change in oil concentration of retentate, relative to feed (%)
A	0.45 ± 0.05	7 ± 2
B	1.1 ± 0.1	1 ± 3
C	1.1 ± 0.2	8 ± 2
D	0.17 ± 0.02	5 ± 7
E	1.4 ± 0.2	10 ± 1
F	1.8 ± 0.3	7 ± 1
G	0.18 ± 0.01	0 ± 2

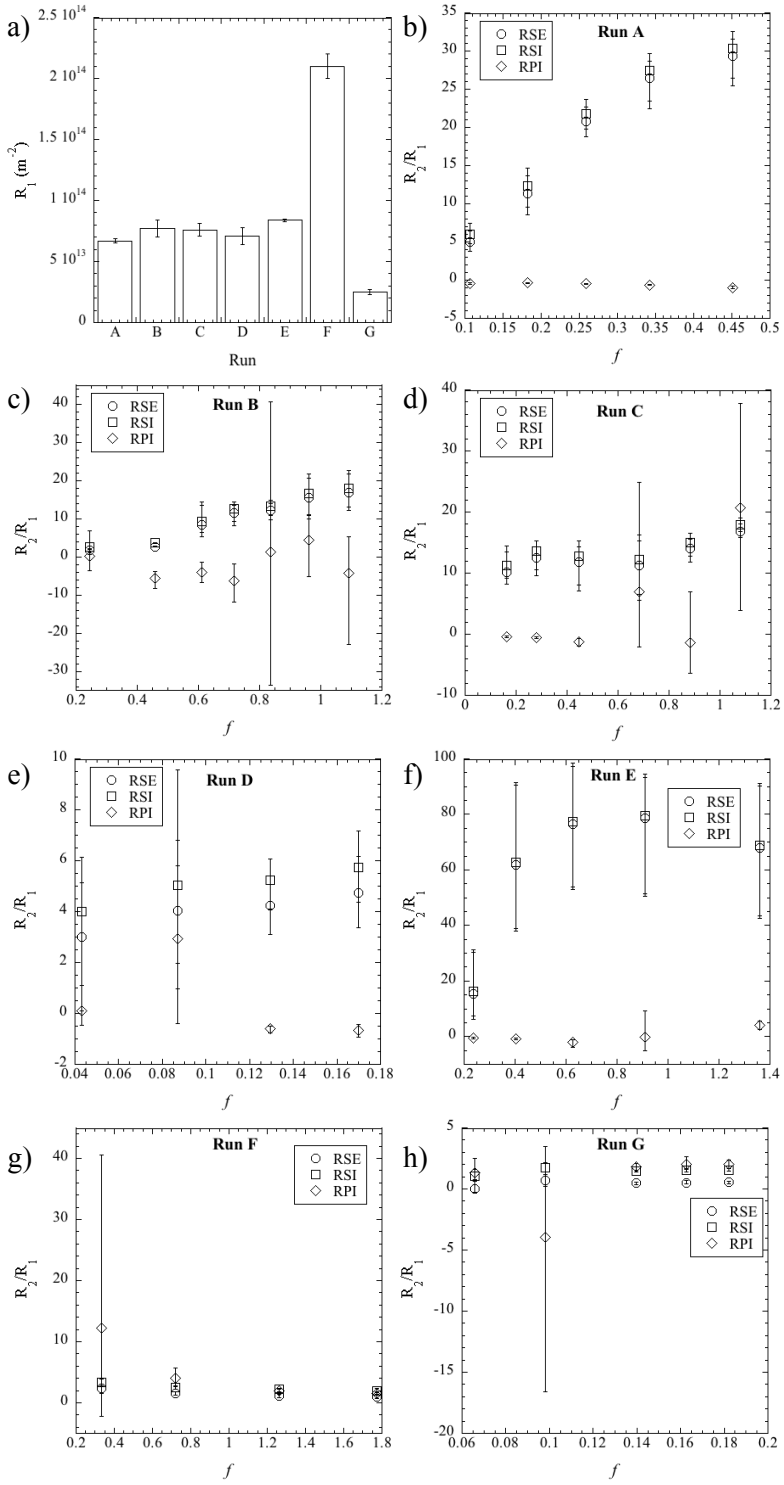

Figure 6 (a) The resistivities of clean membranes, R_1, calculated from the pure water fluxes. (b)-(h) The resistivity ratio R_2/R_1 for each sampling interval for runs A-G, calculated using RSE (circles), RSI (squares), and RPI (diamonds) models.

4.7 CCF Model.

Next, the experimentally measured normalized fluxes are compared with those predicted by the CCF model using Eq. 13, with no adjustable parameters. The effective solidities of the membranes (ϕ) were estimated using $\phi = \phi_0 + f$. The results are shown in Figure 7. The quality of the predicted fluxes is generally as good, or better, than any of the preceding models under the assumption of constant R_2. In runs A through E, the agreement is quantitative, while in runs F and G, the trends are captured while the magnitude of flux is under-predicted. The assumption that the oil component renders a part of the membrane impermeable is supported by the observation that $R_2/R_1 >> 1$ for runs A-E; breakdown of this assumption may be responsible for the poorer performance of this model in runs F and G. Unlike the previous models, the CCF model accounts not only for the change in effective solidity of the membrane due to fouling, but also the perturbation of the flow field through the membrane that arises as the coating on the fibers builds up.

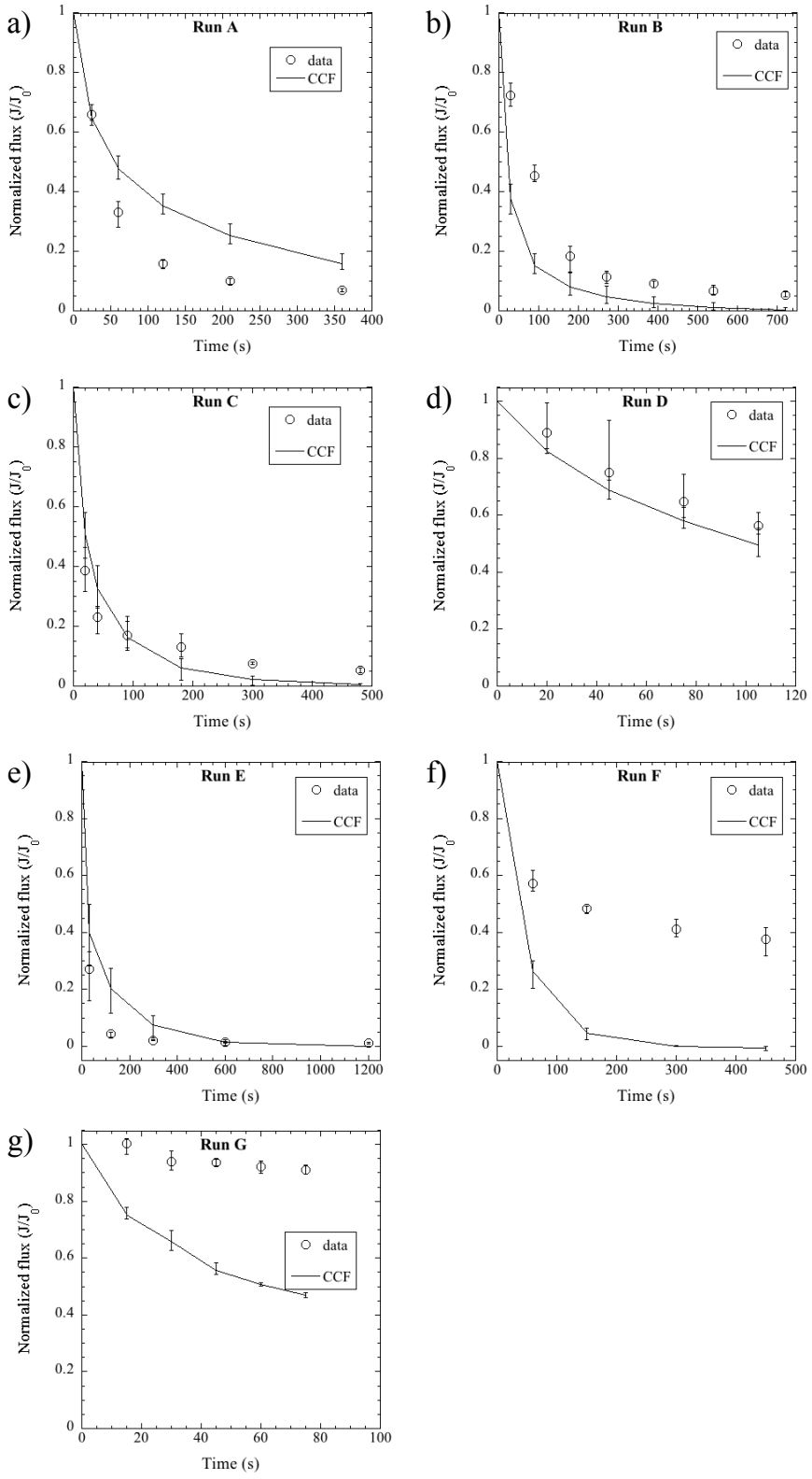

Figure 7 The comparison of the experimental normalized flux vs. time (circles) with that predicted by the CCF model (lines). The error bars on the CCF model were obtained from the maximum and minimum J/J_0 values calculated from all the experimental replicates The R-square

values are 0.79 (run A), 0.93 (run B), 0.85 (run C), 0.8 (run D), 0.96 (run E), -19 (run F) and -176 (run G).

5 Discussion

5.1 Limitation of the Fouling Description

The total amount of foulant retained is characterized by f, which is used in both the resistivity and CCF models. The main assumption in calculating f is that the foulant retained does not get re-suspended into the feed; however, as shown in Table 4, this assumption breaks down for several of the runs (A, C, E and F). It is also evident that f is overestimated ($f > 1$) in several of the same runs (B, C, E and F). However, the breakdown of this assumption does not greatly impair the predictive capability of the models, since as f approaches unity, the flux (including transport of additional oil to the membrane) drops nearly to zero.

In this work, we have assumed that the foulant within the membrane is non-porous (its density is constant) and that its resistivity is intrinsic to the foulant. However, other works have proposed that R_2 depends on such parameters as the droplet diameter and the "solidity" of the foulant layer, ϕ_{oil}, for example [33]:

$$R_2 \propto \frac{\phi_{oil}}{d_p^2\left(1-\phi_{oil}\right)^3}. \qquad (14)$$

The "solidity" of the foulant layer has also been reported to increase with increasing emulsion concentration and polydispersity [34], and with pressure [35, 36]. However, we do not find any pressure dependence in this work, perhaps due to the low range of pressures employed. The resistivity of the foulant component may also depend on coalescence of droplets within the membrane, or upon pore size [36]. In the latter case, a possible explanation is that the packing density of the foulant layer is dependent on the space available as it grows. For the runs with $d_p/d_f = 1.1$ (A-E), the resistivity of foulant is highest because the droplets accumulate within the confined pore space. For run F ($d_p/d_f = 2.5$), the oil droplets are less likely to enter the membrane,

hence a more porous foulant layer builds up external to the membrane. For run G ($d_p/d_f = 0.57$), the droplets accumulate within the pore space of the membrane, but are hardly confined by it.

5.2 Factors affecting separation properties.

The flux of permeate depends on the total effective solidity of a membrane after fouling occurs. The solidity increases more quickly with increasing concentration of dodecane due to more oil droplets available to foul the membrane. However, when $d_p/d_f = 2.5$ (run F), the oil is more likely to accumulate on the surface of the membrane rather than in its interior, thus altering less the effective solidity of the membrane itself. Additionally, when oil accumulates on the surface of the membrane, it is more likely to be re-suspended in the retentate, a conclusion that is supported by the data in Table 4. On the other hand, when $d_p/d_f = 0.57$ (run G), the rejection is lower than in the other runs, and most of the oil droplets pass through membrane without encountering the fibers; in this case, the solidity increases more slowly.

According to Gopal et al., rejection occurs in one of two ways when the particles are solid: size exclusion if $d_p/d_f > 2$, or adsorption within the membrane if $d_p/d_f < 2$ [9]. However, our results for liquid emulsions suggest that there might be internal fouling even for $d_p/d_f = 2.5$ (run F). The difference is probably due to the deformability of the fluid oil droplets, which permits them to enter the membrane and wet out on the fibers, thus causing internal fouling even at high d_p/d_f (>2).

The emulsion size results (Table 2) show significant growth of the droplet size in the permeate in runs A (P = 2 psi) and B (P = 1 psi), indicating that some coalescence occurs. By contrast, the significant decrease in droplet size in the permeate for runs C (P = 4 psi) and F ($d_p/d_f = 2.5$) is attributed to the break up of droplets. The reduction in droplet size could be due to the higher stresses experienced by the droplets in these runs, due to higher flux (run C) and smaller pore size (run F).

6 Conclusions

In summary, the microfiltration of oil-in-water emulsions with droplet diameters around 250 nm using electrospun fiber membranes is reported. The performances of the membranes are examined as functions of flux (applied pressure), oil concentration and fiber size within the membranes. In every case, the flux declines with time due to fouling of the membrane with the oil. Comparison to a commercial membrane of comparable nominal pore size (bubble point) indicates that the rejection achieved by the electrospun membranes is comparable to the commercial membrane, but that the flux is several times higher. These observations indicate that electrospun membranes may be promising as microfilters for emulsified liquids.

Several models are presented to characterize the effect of fouling on performance for the electrospun membranes. The MFI model is shown to be one of a class of models based on simple assumptions of series or parallel resistances to flow through the membrane. Referred to here as the RSE model, it does a good job of describing the reduction in flux due to fouling of the membrane by oil. This model supports the assumption that the resistivity of the oil is one to two orders of magnitude greater than that of the membrane itself, and may therefore be considered "impermeable". Discrepancies with this model can be attributed to a breakdown of certain assumptions, for example the re-suspension of oil from the membrane surface to the retentate and the coalescence of the oily regions that form upon or within the membrane. From the models we conclude that the foulants contributed to the overall resistance to flow in series with the membrane resistance. The rejection mechanism was likely to transition from adsorption (internal fouling) to size exclusion (external fouling) as the effective fiber diameter grew with filtration time.

A more physically-motivated model called the Conformally Coated Fibers (CCF) model is proposed for fouling of fibrous material like the electrospun membranes examined in this work. This model assumes that the foulant is impermeable and that it wets out on the fibers rather than blocking the pores, as would be the case for solid particles. Since it is based on Happel's model for flow around a fiber, it accounts for changes in hydrodynamics as the coated fibers increase in diameter. This model captures qualitatively, in some cases quantitatively, the decline in flux with fouling of the membranes reported in this work, and does not require any adjustable

parameters. Its utility may reach beyond that of the electrospun fiber membranes and oil-in-water emulsion separations reported in this work.

Acknowledgement

Funding for this project was provided by King Fahd University of Petroleum and Minerals (KFUPM) in Dhahran, Saudi Arabia, through the Center for Clean Water and Clean Energy at MIT and KFUPM under PROJECT NUMBER R5-CW-08, and by the Cooperative Agreement between the Masdar Institute of Science and Technology (Masdar University), Abu Dhabi, UAE and the Massachusetts Institute of Technology (MIT), Cambridge, MA, USA, Reference No. 02/MI/MI/CP/11/07633/GEN/G/00". We would also like to acknowledge the Institute for Soldier Nanotechnology at MIT for use of facilities.

References

[1] M. Cheryan, N. Rajagopalan, Membrane processing of oily streams, wastewater treatment and waste reduction, Journal of Membrane Science 151 (1998) (1) 13-28.

[2] J. K. Milic, A. Muric, I. Petrinic, M. Simonic, Recent developments in membrane treatment of spent cutting-oils: A review, Industrial & Engineering Chemistry Research 52 (2013) 7603-7616

[3] F.R. Ahmadun, A. Pendashteh, L.C. Abdullah, D.R.A. Biak, S. S. Madaeni, Z.Z. Abidin, Review of technologies for oil and gas produced water treatment, Journal of Hazardous Materials 170 (2009) 530-551.

[4] A. Salahi, T. Mohammadi, A.R. Pour, F. Rekabdar, Oily wastewater treatment using ultrafiltration, Desalination and Water Treatment 6 (2009) 289-298.

[5] B. Chakrabarty, A.K. Ghoshal, M.K. Purkait, Ultrafiltration of stable oil-in-water emulsion by polysulfone membrane, Journal of Membrane Science 325 (2008) 427-437.

[6] P. Gibson, H. Schreuder-Gibson, C. Pentheny, Electrospinning technology: Direct application of tailorable ultrathin membranes, Journal of Coated Fabrics 28 (1998) 63-72.

[7] K. Yoon, K. Kim, X. Wang, D. Fang, B.S. Hsiao, B. Chu, High flux ultrafiltration membranes based on electrospun nanofibrous PAN scaffolds and chitosan coating, Polymer 47 (2006) 2434-2441.

[8] R. Gopal, S. Kaur, Z. Ma, C. Chan, S. Ramakrishna, T. Matsuura, Electrospun nanofibrous filtration membrane, Journal of Membrane Science 281 (2006) 581-586.

[9] R. Gopal, S. Kaur, C.Y. Feng, C. Chan, S. Ramakrishna, S. Tabe, T. Matsuura, Electrospun nanofibrous polysulfone membranes as pre-filters: Particulate removal, Journal of Membrane Science 289 (2007) 210-219.

[10] Z. Tang, J. Wei, L. Yung, B. Ji, H. Ma, C. Qiu, K. Yoon, UV-cured poly(vinyl alcohol) ultrafiltration nanofibrous membrane based on electrospun nanofiber scaffolds, Journal of Membrane Science 328 (2009) 1-5.

[11] K. Yoon, B. S. Hsiao, B. Chu, High flux ultrafiltration nanofibrous membranes based on polyacrylonitrile electrospun scaffolds and crosslinked polyvinyl alcohol coating, Journal of Membrane Science 338 (2009) 145-152.

[12] S. S. Homaeigohar, K. Buhr, K Ebert, Polyethersulfone electrospun nanofibrous composite membrane for liquid filtration, Journal of Membrane Science 365 (2010) 68-77.

[13] A. Patanaik, V. Jacobs, R. D. Anandjiwala, Performance evaluation of electrospun nanofibrous membrane, Journal of Membrane Science 352 (2010) 136-142.

[14] X. Wang, K. Zhang, Y. Yang, L. Wang, Z. Zhou, M. Zhu, B. S. Hsiao, B. Chu, Development of hydrophilic barrier layer on nanofibrous substrate as composite membrane via a facile route, Journal of Membrane Science 356 (2010) 110-116.

[15] H. Ma, C. Burger, B.S. Hsiao, B. Chu, Ultrafine polysaccharide nanofibrous membranes for water purification, Biomacromolecules 12 (2011) (4) 970-976.

[16] H. You, Y. Yang, X. Li, K. Zhang, X. Wang, M. Zhu, Low pressure high flux thin film nanofibrous composite membranes prepared by electrospraying technique combined with solution treatment, Journal of Membrane Science 394-395 (2012) 241-247.

[17] R. Wang, Y. Liu, B. Li, B.S. Hsiao, B. Chu, Electrospun nanofibrous membranes for high flux microfiltration, Journal of Membrane Science 392-393 (2012) 167-

174.

[18] L.T. Choong, Z. Khan, G.C. Rutledge, Permeability of electrospun fiber membranes under hydraulic flow, Journal of Membrane Science 451 (2014) 111-116.

[19] K. Yoon, B. Hsiao, B. Chu, Functional nanofibers for environmental applications, Journal of Materials Chemistry 18 (2008) 5326-5334.

[20] B. Lalia, E. Guillen, H. Arafat, R. Hashaikeh, Nanocrystalline cellulose reinforced PCDF-HFP membranes for membrane distillation application, Desalination 332 (2014) 134-141.

[21] R.D. Noble, S.A. Stern, Membrane Separations Technology: Principle and Applications, Elsevier, New York, 1995, Ch. 2.

[22] W.R. Bowen, J.I. Calvo, A. Hernandez, Steps of membrane blocking in flux decline during protein microfiltration, Journal of Membrane Science 101 (1995) 153-165, and references therein.

[23] J. Hermia, Constant pressure blocking filtration laws – Application to power law non-newtonian fluids, Transactions of the Institution of Chemical Engineers 60 (1982) 183-187.

[24] C. Tien, B.V. Ramarao, Revisiting the laws of filtration: An assessment of their use in identifying particle retention mechanisms in filtration, Journal of Membrane Science 383 (2011) 17-25.

[25] J.C. Schippers, J. Verdouw, The modified fouling index, a method of determining the fouling characteristics of water, Desalination 32 (1980) 137-148.

[26] S. Boerlage, M.D. Kennedy, M.P. Aniye, E. Abogrean, Z.S. Tarawneh, J.C. Schippers, The MFI-UF as a water quality test and monitor, Journal of Membrane Science 211 (2003) 271-289.

[27] H. Huang, T.A. Young, J.G. Jacangelo, Unified membrane fouling index for low pressure membrane filtration of natural waters: Principle and methodology, Environmental Science Technology 42 (2008) 714-720.

[28] R.W. Field, D. Wu, J.A. Howell, B.B. Gupta, Critical flux concept for microfiltration fouling, Journal of Membrane Science 100 (1995) 259-272.

[29] J. Happel, Viscous flow relative to arrays of cylinders, AIChE Journal 5 (1959) 174-177.

[30] S.J. Eichhorn, W.W. Sampson, Statistical geometry of pores and statistics of porous nanofibrous assemblies, Journal of The Royal Society Interface 2 (2005) 309-318.

[31] J.L. Lowery, N. Datta, G.C. Rutledge, Effect of fiber diameter, pore size and seeding method on growth of human dermal fibroblasts in electrospun poly(ε-caprolactone) fibrous mats, Biomaterials 31 (2010) 491-504.

[32] Q.P. Pham, U. Sharma, A.G. Mikos, Electrospun poly(ε-caprolactone) microfiber and multilayer nanofiber/microfiber scaffolds: Characterization of scaffolds and measurement of cellular infiltration, Biomacromolecules 7 (10) (2006) 2796-2805.

[33] R. Baker, A.G. Fane, C. Fell, B. Yoo, Factors affecting flux in crossflow filtration, Desalination 53 (1985) 81-93.

[34] H. Y. Sohn, C. Moreland, The effect of particle size distribution on packing density, The Canadian Journal of Chemical Engineering 46 (1968) 162-167.

[35] T. Kawakatsu, S. Nakao, S. Kimura, Effects of size and compressibility of suspended particles and surface pore size of membrane on flux in crossflow filtration, Journal of Membrane Science 81 (1993) 173-190.

[36] E. Tracey, R. Davis, Protein fouling of track-etched polycarbonate microfiltration membranes, Journal of Colloid and Interface Science 167 (1994) 104-116.